PIER C

(Received 23 May 2025, Accepted 15 October 2025, Scheduled 26 December 2025)

RCS Reduction Technology for Circularly Polarized Satellite Navigation Antenna Based on Phase Gradient Surface

Lei Gan[1], Kun Wei[2,*], Jing-Xian Chen[1], and Qing-Chao Guo[1]

[1] *Shenyang Aircraft Design and Research Institute, Shenyang, China*
[2] *National Key Laboratory of Radar Detection and Sensing, Xidian University, Xi'an 710071, Shaanxi, China*

ABSTRACT: With the advancement of radar detection technology, stealth technology has become increasingly critical in modern warfare. Antennas, as essential components of airborne platforms, are significant scattering sources on stealth aircraft. This paper proposes a method to reduce the Radar Cross Section (RCS) of B3-band satellite navigation antennas using a broadband phase gradient surface. The phase gradient surface is designed to deflect scattered energy into non-threatening angular domains, thereby achieving RCS reduction. The proposed design is validated through simulation software, demonstrating its effectiveness in reducing RCS while maintaining the radiation performance of the antenna. The results show that the phase gradient surface can achieve more than 4 dB and 6 dB of RCS reduction under phi- and theta-polarized plane wave incidence, respectively, in the frequency range of 5.5 GHz to 15 GHz.

1. INTRODUCTION

With the development of radar detection technology, stealth technology is becoming increasingly important in modern warfare. Antennas, as an essential part of airborne platforms, are an important scattering source on stealth aircraft. Therefore, antenna stealth technology has become a key issue in aircraft stealth technology. Traditional stealth technologies are mainly divided into four categories: shaping technology, radar absorbing materials, passive cancellation technology, and active cancellation technology. Over the years, many researchers have conducted in-depth research on these four technologies and achieved certain results.

Electromagnetic metamaterials, as periodic structures with special electromagnetic properties, have very broad application prospects in antenna stealth technology. Phase gradient surface regulates the beam of scattered electromagnetic waves through a quasiperiodic array structure and avoids the scattered energy to the nonthreatening angle domain, which can achieve RCS reduction of the antenna. In 2011, a phase gradient surface was first proposed using a V-shaped antenna, which achieved phase gradient changes by changing the opening size and rotation direction of the V-shaped structure, thereby altering the direction of scattered electromagnetic waves [1].

In [2], a polarization insensitive phase gradient surface was designed based on efficient artificial surface plasmon coupling, which achieved the deflection (bandwidth) of any linearly polarized incident wave through a centrally symmetric arrangement. Refs. [3–5] designed a wideband angular domain encoded phase gradient surface based on Pancharatnam-Berry phase. Ref. [6] implemented the design of a broadband phase gradient surface using a 2-bit encoded phase gradient surface. For phase gradient surfaces, Refs. [7, 8] achieved backscattering suppression within broadband by optimizing the arrangement. In [9], a double resonant unit capable of achieving 360° phase shift was selected to design a randomly arranged phase gradient surface, achieving wideband RCS reduction. The use of phase gradient surface transmission waveguide mode in [10] reduces the transmission loss of high-frequency microstrip lines. In [11], wide angle RCS reduction was achieved by randomly arranging units with different reflection phases. Ref. [12] used a hybrid resonant structure to achieve phase gradient surfaces at two frequency points, achieving dual frequency RCS reduction.

However, currently phase gradient surfaces are mostly used for RCS reduction of metal plates and are less commonly used for RCS reduction of antennas [13, 14]. In [13], a broadband -10 dB RCS reduction was achieved by loading a randomly arranged phase gradient surfaces onto a metallic ground plane. In [14], broadband RCS reduction of a metallic ground plane was achieved by employing two different phase gradient surfaces. In [15], the phase gradient surface was combined with an F-P resonant cavity antenna structure to design a stealth coating structure, achieving in band RCS reduction of the F-P resonant cavity antenna. The limited application of phase gradient surfaces in antenna stealth technology is mainly due to their narrow bandwidth, polarization, and angle sensitivity. This paper proposes corresponding solutions to address the two disadvantages of phase gradient surfaces and applies the designed phase gradient surface to RCS reduction of slot array antennas. The effectiveness of this approach is verified using simulation software.

2. THEORY OF PHASE GRADIENT SURFACE

Phase gradient surface is an anisotropic artificial surface with approximately zero thickness, composed of metal unit struc-

* Corresponding author: Kun Wei (weikun@xidian.edu.cn).

tures approximately arranged in subwavelength sizes. The phase gradient surface can control the propagation direction of electromagnetic waves, and its working mechanism follows the generalized laws of reflection and refraction (generalized Snell's law).

As shown in Figure 1, for a uniform interface, the incident wave is θ_i incident on the interface at an incident angle, and its reflection angle is θ_r. The incident angle is equal to the reflection angle $\theta_i = \theta_r$. In the two-dimensional plane, the reflected wave vector k_r can be expressed as the k_{rz} vector k_{rz} sum k_r of $k_{rx}k_{rx}$ and $k_r = k_{rx} + k_{rz}$, where and represent the x and z components, respectively. However, considering the interface between the phase gradient surface and air, the incident electromagnetic wave can be reflected to an expected angle θ_{ar}. To simplify the formula without loss of generality, it is assumed that the phase gradient surface exhibits a gradient change in reflected phase along the x-direction. Heterogeneous reflection is achieved by phase gradient $\xi = d\phi/dx = \Delta\phi/np$, where p represents the period of the phase gradient surface; n represents the number of elements; and N elements are arranged in a subarray periodically to achieve a 360° phase change. The phase difference between adjacent elements $\Delta\phi$ is constant, achieving a fixed phase shift in the x-direction.

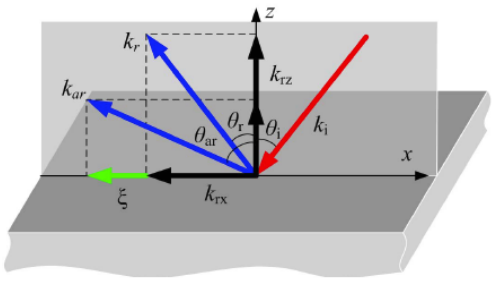

FIGURE 1. Schematic diagram of the reflection and refraction model.

Considering the phase gradient, Snell's law of reflection/refraction can be expressed as

$$k_{ar} \sin\theta_{ar} = k_r \sin\theta_r \pm \xi = k_{rx} \pm \xi \tag{1}$$

The representation $\pm$ here is the same or opposite to the x-axis direction. k_0 represents the wave vector of the incident wave in free space. It can be seen that in free space $k_i = k_0 = k_r$, the angle of anisotropic reflection θ_{ar} can be expressed as

$$\theta_{ar} = \arcsin\frac{k_{rx} + \xi}{k_0} \tag{2}$$

Under normal incidence, $k_{rx} = 0$; therefore, the aforementioned equation can be expressed as

$$\theta_{ar} = \arcsin\frac{\xi}{k_0} \tag{3}$$

If the unit cell period of the phase-gradient metasurface is p and the phase shift within a unit cell approximately 2π, the phase gradient is given by $\xi = 2\pi/p$. The anomalous reflection angle can then be calculated as follows:

$$\theta_{ar} = \arcsin\frac{\lambda}{p} \tag{4}$$

Therefore, the ratio of the wavelength to the period size, $\xi/k_0 = \lambda/p$, plays a decisive role in determining the anomalous reflection angle. Hence, by tailoring the relationship between the period of the phase-gradient metasurface and operating wavelength, arbitrary steering of the scattered beam can be achieved.

3. BROADBAND PHASE GRADIENT SURFACE ELEMENT DESIGN

This article designs a broadband phase gradient surface element structure with a center frequency of 10 GHz. Initially, a square-loop structure is adopted as the unit element of the phase gradient surface (PGM). The reflection phase response of this element is illustrated in Figure 2(a). It can be observed that as the frequency increases, the phase curves converge, making it difficult to maintain a stable phase gradient. To address this issue, a metal circular ring and two orthogonal metallic strips at the center of the circular square ring are incorporated inside the square loop. The corresponding reflection phase performance of the modified unit is shown in Figure 2(b). As demonstrated, the reflection phase under various geometric parameters maintains a consistent gradient across frequency, thereby satisfying the requirements for broadband PGM design.

As shown in Figure 3, the proposed unit structure consists of three layers, with the first layer being a metal layer printed with a phase gradient surface unit structure, the middle layer being a 3 mm thick FR4 dielectric substrate with $\tan\delta = 0.02$, and the bottom layer being a metal reflector. This structure utilizes a combination of ring structure and oscillator structure, allowing different unit structures to maintain approximate phase differences over a wide frequency band. The period of the unit structure is close to the half medium wavelength $p = 12$ mm in the low-frequency range. The side length of the square ring is $wp_1 = 6.5$ mm, and the width is d_1. The outer diameter of the circular ring is $r_3 = 4.5$ mm, and the inner diameter is $r_4 = 4$ mm. The length of the internal cross oscillator is $2 * r_3$, and the width $d_2 = 0.5$ mm.

The unit structure proposed here utilizes a combination of ring and oscillator structures to achieve broadband phase change. The imaginary part of the impedance of the ring antenna is inductive, while the imaginary part of the impedance of the oscillator antenna is capacitive, forming an LC resonant structure that can achieve continuous phase change in a wide frequency band. To demonstrate our design concept, the above unit structure was simulated using the infinite periodic boundary conditions of full wave simulation software HFSS15.0 to calculate S-parameters of the unit. Master-slave boundary conditions were set along x and y directions, and the plane incident waves of x polarization and y polarization propagated from the $+z$ direction to the $-z$ direction. Figure 4 shows the reflection coefficient curve of the phase gradient surface element in the 5–15 GHz frequency band. It can be seen that the designed phase gradient surface has three resonance points, corresponding to the square ring, circular ring, and oscillator structure in the physical structure. The three resonance points make the unit structure have a stable phase change with frequency. The first two resonance points have smaller losses,

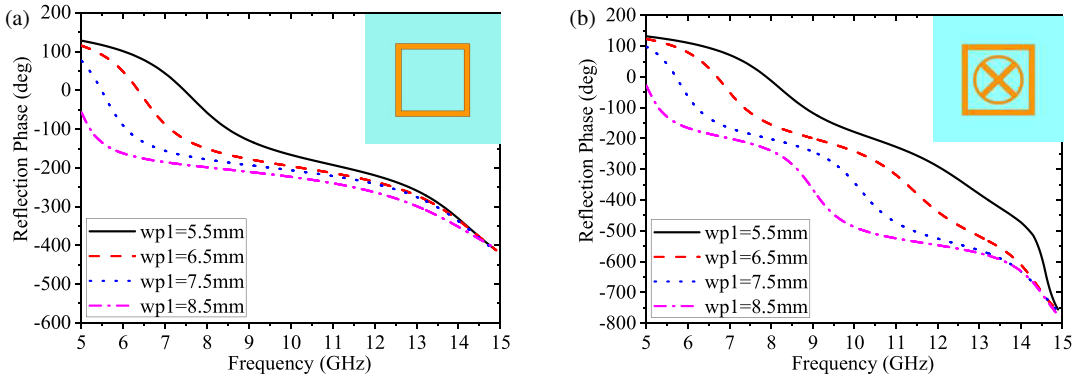

FIGURE 2. Reflection phase of the unit cells with different length of wp_1. (a) Only a square-loop. (b) Square-loop with a metal circular ring and two orthogonal metallic strips.

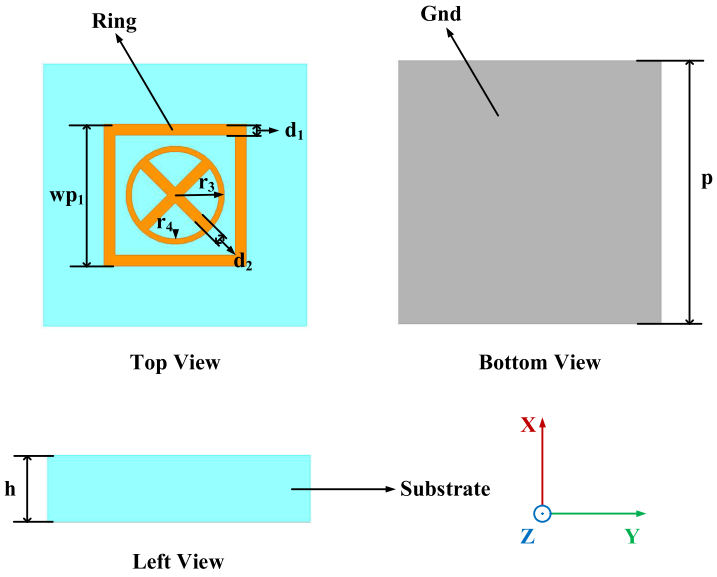

FIGURE 3. Three-views of unit cell.

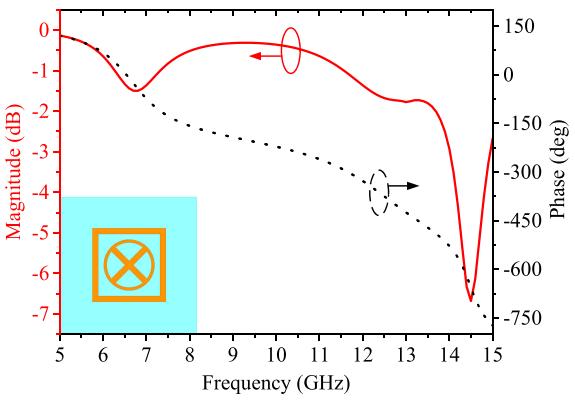

FIGURE 4. Reflection coefficient curve of phase gradient surface element.

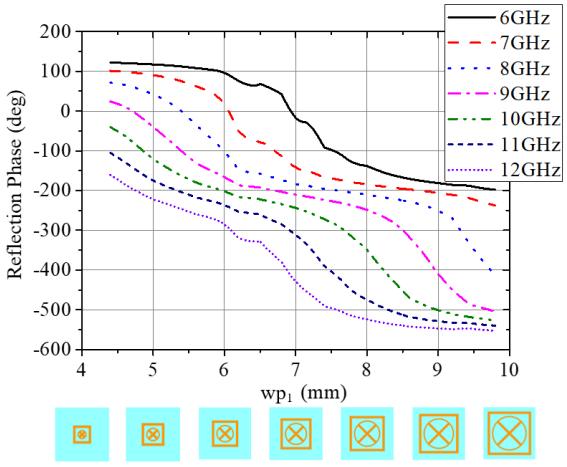

FIGURE 5. Phase curves of different units at different frequencies.

corresponding to the ring structure, and the oscillator structure, which is a strong resonance structure, corresponds to the last resonance point.

Figure 5 shows the phase variation curves of different units at different frequencies. It can be seen that as the size changes, the reflection phase of units above 8 GHz can cover 360°. The reflection phase change in the frequency band below 8 GHz is achieved by the outermost square ring, so its reflection phase can only cover 300°. In order to fully utilize the reflection phase of the unit and avoid errors caused by incomplete coverage of

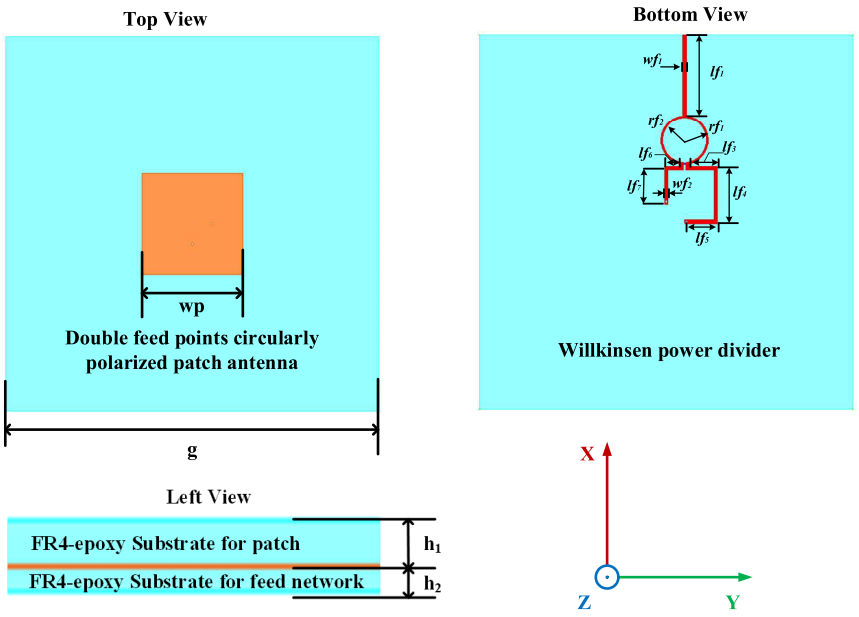

FIGURE 6. Model diagram of circularly polarized microstrip antenna.

TABLE 1. Parameters of the designed circularly polarized feeding structure.

Dimension	Value (mm)	Dimension	Value (mm)
wf_1	2.4	wf_2	2.4
lf_1	43.2	lf_3	15.4
lf_4	29.4	lf_5	16.5
lf_6	8.2	lf_7	18.0
rf_1	13.6	rf_2	12.5

360° by units below 8 GHz, the phase gradient can be determined as 60°, and the reflection phase curve at 10 GHz can be fitted using a binomial function.

$$\text{Reflection Phase} = 0.768wp_1^3 - 20.748wp_1^2 + 84.867wp_1 - 111.518 \quad (5)$$

Equation (5) establishes the relationship between unit size and reflection phase. For the reflection phase at any position on the phase gradient surface, the corresponding unit size can be calculated based on Equation (5), achieving the correspondence between mathematical and physical models.

4. DESIGN OF CIRCULARLY POLARIZED SATELLITE NAVIGATION ANTENNA

Circularly polarized microstrip antennas can be divided into singly fed circularly polarized microstrip antennas and doubly fed circularly polarized microstrip antennas according to the feeding method. In this paper, the double fed method is used to design circularly polarized antennas. The doubly fed circularly polarized microstrip antenna utilizes a phase difference of 90° between two feeding points to achieve circularly polarized operation.

Compared to a singly fed circularly polarized antenna, the axis ratio of the doubly fed circularly polarized antenna is closer to 1 and has a wider bandwidth. Therefore, in this paper, a circularly polarized microstrip antenna operating in the B3 band (1246 MHz–1256.5 MHz) is designed using doubly fed method. Figure 6 shows the model diagram of a circularly polarized microstrip antenna fed by a Wilkinson power divider. The detailed parameters of the designed circularly polarized feeding structure are summarized in Table 1. By adjusting the lengths of phase-shift lines in two orthogonal polarization directions, a 90° phase difference is introduced between the x- and y-polarizations, resulting in a right-hand circularly polarized (RHCP) beam. This design is suitable for satellite communication applications.

5. DESIGN OF LOW RCS CIRCULARLY POLARIZED SATELLITE NAVIGATION ANTENNA

The satellite antenna installed on the aircraft is a strong scattering source on stealth aircraft. In this paper, a broadband phase gradient surface is designed for enemy radar detection bands, which is integrated with a circularly polarized microstrip antenna to achieve the design of a low RCS B3 band satellite navigation antenna. Figure 7 shows the integrated design model of phase gradient surface and microstrip antenna. Figure 8 shows the fabricated phase gradient surface and antenna.

In order to verify the radiation and scattering performance of the antenna designed in this study, processing tests were conducted on the satellite navigation antenna loaded with a phase gradient surface. Figure 9 shows the comparison results of S_{11} between the designed antenna and reference antenna. It can be seen that there is not much difference in the simulation results of S_{11} between the designed antenna and reference antenna. However, there is a difference between the simulated and tested S_{11} of the designed antenna. The -10 dB bandwidth of test results has narrowed, but it still covers the B3 band. Therefore, it can

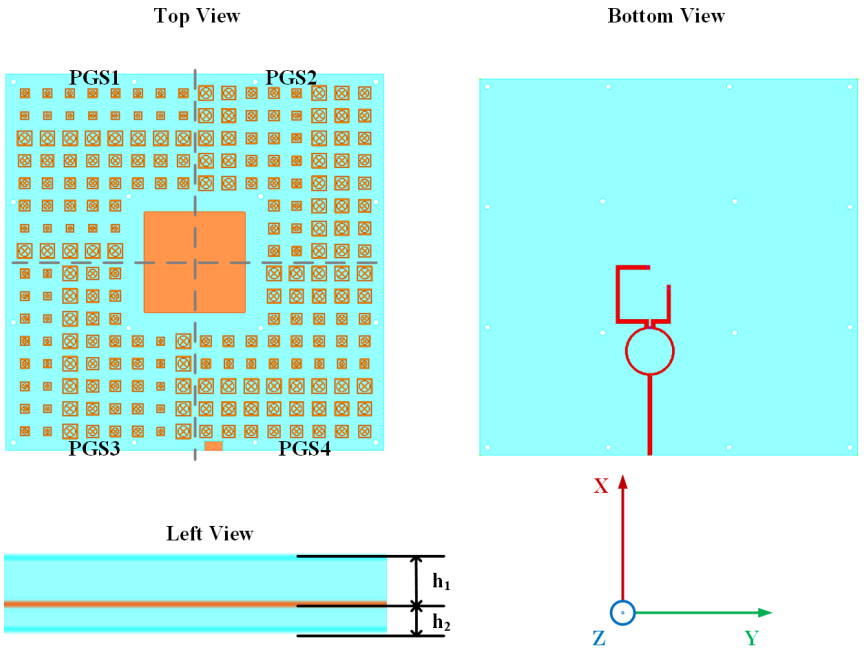

FIGURE 7. Integrated design model of phase gradient surface and microstrip antenna.

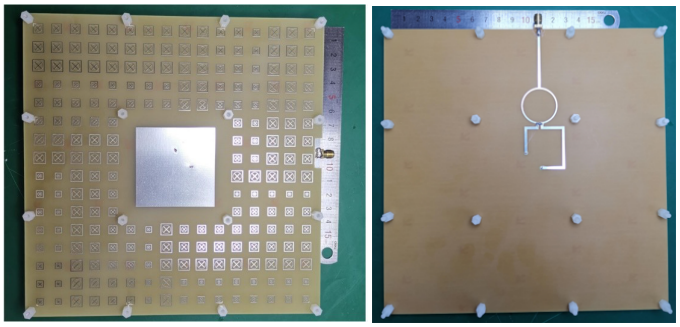

FIGURE 8. Physical image of loading phase gradient surface microstrip antenna.

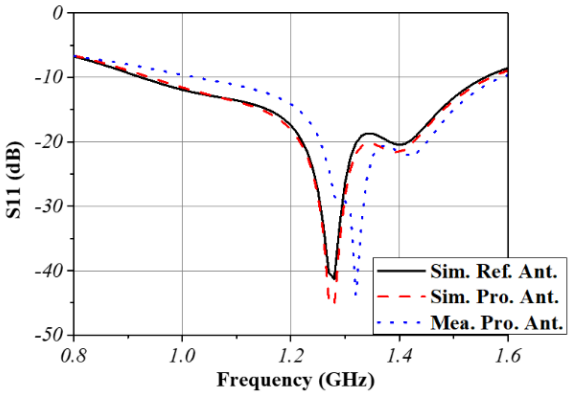

FIGURE 9. Return loss diagram of antenna.

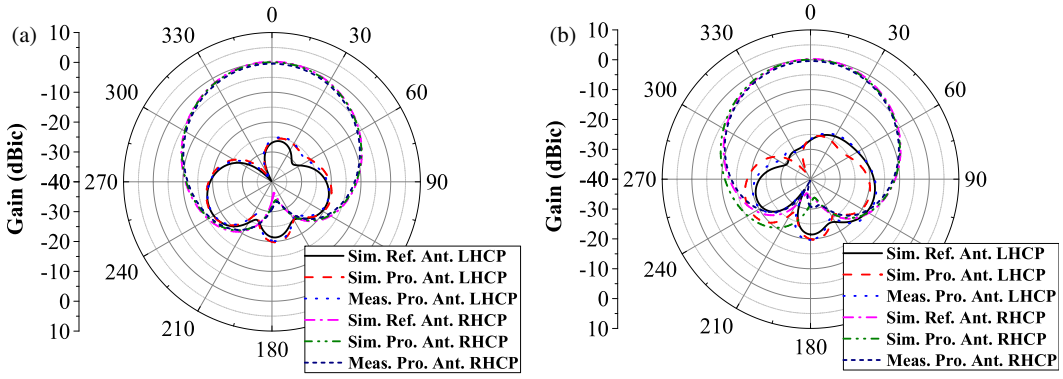

FIGURE 10. Directional diagram at 1250.618 MHz frequency point. (a) *xoz* plane, (b) *yoz* surface.

be considered that the resonant frequency points of the simulation and test results are basically consistent, and the bandwidth difference is not significant. Figures 10–12 show the simulation results of the E-plane and H-plane directional patterns of the designed antenna and reference antenna. The directional patterns of the B3 band at 1250.618 MHz and 1286.423 MHz are basically consistent. Compared with the reference antenna, the loading of the phase gradient surface causes the right-handed

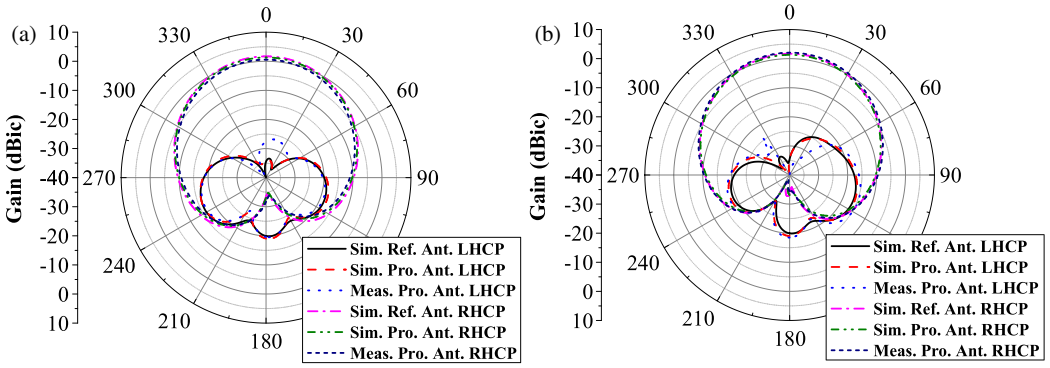

FIGURE 11. Directional diagram at the center frequency point of 1268 MHz. (a) *xoz* surface, (b) *yoz* surface.

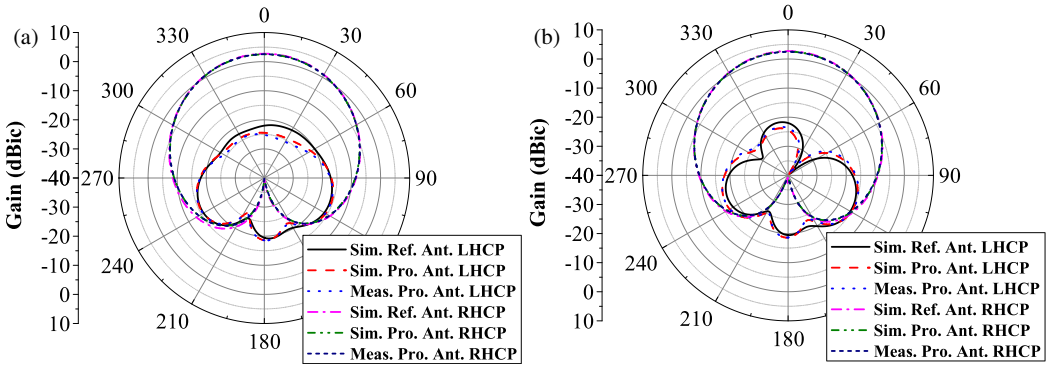

FIGURE 12. Direction diagram at 1286.423 MHz frequency point. (a) *xoz* surface, (b) *yoz* surface.

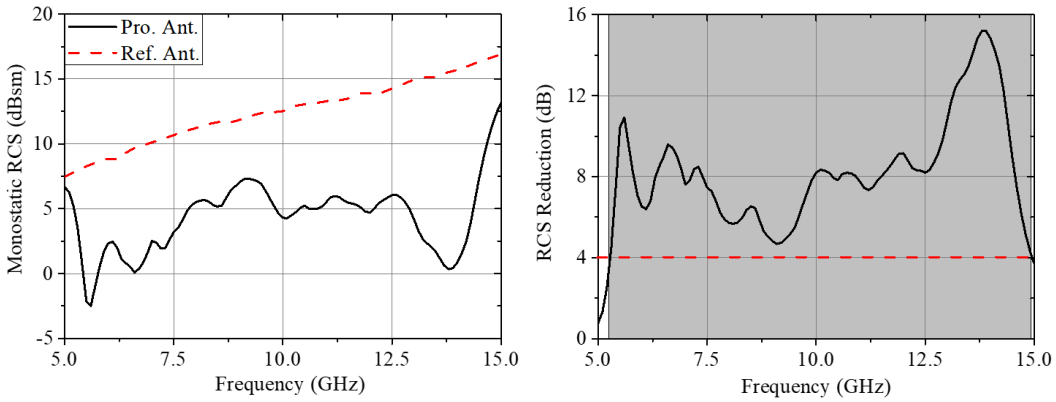

FIGURE 13. Comparison of phi polarized single station RCS between design antenna and reference antenna.

circular polarization gain of the antenna to remain unchanged, but the cross-polarization level slightly decreases. Overall, the loading of phase gradient surfaces has little effect on the radiation performance of antennas. The directional patterns of the reference antenna and designed antenna at the center frequency of 1268 MHz in the B3 band are basically the same, but the gain of the designed antenna has decreased by about 0.6 dB, and the cross-polarization level remains unchanged.

Figures 13 and 14 show the simulation results of the single station RCS of the designed antenna and reference antenna. It can be seen that in the frequency range of 5.5 GHz–15 GHz, compared with the reference antenna, the single station RCS of the designed antenna is reduced by more than 4 dB under phi polarized plane wave incident state and by more than 6 dB under theta polarized plane wave incident state.

Finally, a comparison between the proposed design and existing works employing phase-gradient metasurfaces is presented in Table 2. The results demonstrate that the proposed design exhibits the following advantages:

1. It achieves circularly polarized radiation in the B3 band for satellite communication;
2. It realizes ultra-wideband scattering reduction from 5 to 15 GHz;
3. The antenna features a low-profile structure, facilitating its integration into various satellite communication platforms.

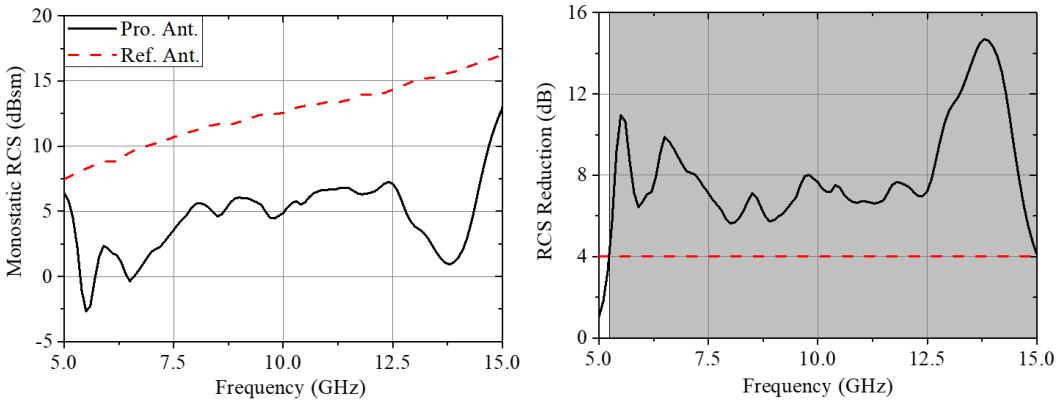

FIGURE 14. Comparison of theta polarized single station RCS between designed antenna and reference antenna.

TABLE 2. A comparison between the proposed design and existing works.

Ref.	Size	Center Frequency (GHz)	RCS Reduction Bandwidth (dB)	Circular Polarization Performance
[5]	$1.56\lambda_0 \times 1.56\lambda_0 \times 0.15\lambda_0$	15	8–22(93%)	N/A
[13]	$10.5\lambda_0 \times 10.5\lambda_0 \times 0.07\lambda_0$	11	5.3–18(109%)	N/A
[15]	$3.36\lambda_0 \times 3.36\lambda_0 \times 0.70\lambda_0$	8.4	7–16(78%)	N/A
[16]	$1.82\lambda_0 \times 2.42\lambda_0 \times 0.30\lambda_0$	7	4–13(105.8% VP) 5.2–13(85.7% HP)	N/A
[17]	$1.7\lambda_0 \times 1.7\lambda_0 \times 0.40\lambda_0$	4.3	3.5–5(35.3%)	N/A
This work	$0.9\lambda_0 \times 0.9\lambda_0 \times 0.012\lambda_0$	1.25	5–15(100%)	RHCP

6. CONCLUSION

This article proposes a method of using phase gradient surfaces to reduce the RCS of B3 band satellite navigation antennas. The medium plate of the satellite navigation antenna is divided into four regions, and the gradient direction of each region is not consistent, so that the scattered energy scatters in four directions, achieving RCS reduction of the satellite navigation antenna. The design in this paper provides a new idea for the arrangement of phase gradient surfaces.

REFERENCES

[1] Yu, N., P. Genevet, M. A. Kats, F. Aieta, J.-P. Tetienne, F. Capasso, and Z. Gaburro, "Light propagation with phase discontinuities: Generalized laws of reflection and refraction," *Science*, Vol. 334, No. 6054, 333–337, 2011.

[2] Wu, C., Y. Cheng, W. Wang, B. He, and R. Gong, "Ultra-thin and polarization-independent phase gradient metasurface for high-efficiency spoof surface-plasmon-polariton coupling," *Applied Physics Express*, Vol. 8, No. 12, 122001, 2015.

[3] Zheng, Q., Y. Li, J. Zhang, H. Ma, J. Wang, Y. Pang, Y. Han, S. Sui, Y. Shen, H. Chen, and S. Qu, "Wideband, wide-angle coding phase gradient metasurfaces based on Pancharatnam-Berry phase," *Scientific Reports*, Vol. 7, No. 1, 43543, 2017.

[4] Li, Y., J. Zhang, S. Qu, J. Wang, H. Chen, L. Zheng, Z. Xu, and A. Zhang, "Achieving wideband polarization-independent anomalous reflection for linearly polarized waves with dispersionless phase gradient metasurfaces," *Journal of Physics D: Applied Physics*, Vol. 47, No. 42, 425103, 2014.

[5] Feng, M., Y. Li, Q. Zheng, J. Zhang, Y. Han, J. Wang, H. Chen, S. Sai, H. Ma, and S. Qu, "Two-dimensional coding phase gradient metasurface for RCS reduction," *Journal of Physics D: Applied Physics*, Vol. 51, No. 37, 375103, 2018.

[6] Liang, L., M. Wei, X. Yan, D. Wei, D. Liang, J. Han, X. Ding, G. Zhang, and J. Yao, "Broadband and wide-angle RCS reduction using a 2-bit coding ultrathin metasurface at terahertz frequencies," *Scientific Reports*, Vol. 6, No. 1, 39252, 2016.

[7] Zhang, Y., L. Liang, J. Yang, Y. Feng, B. Zhu, J. Zhao, T. Jiang, B. Jin, and W. Liu, "Broadband diffuse terahertz wave scattering by flexible metasurface with randomized phase distribution," *Scientific Reports*, Vol. 6, No. 1, 26875, 2016.

[8] Wang, K., J. Zhao, Q. Cheng, D. S. Dong, and T. J. Cui, "Broadband and broad-angle low-scattering metasurface based on hybrid optimization algorithm," *Scientific Reports*, Vol. 4, No. 1, 5935, 2014.

[9] Zhuang, Y., G. Wang, J. Liang, T. Cai, X.-L. Tang, T. Guo, and Q. Zhang, "Random combinatorial gradient metasurface for broadband, wide-angle and polarization-independent diffusion scattering," *Scientific Reports*, Vol. 7, No. 1, 16560, 2017.

[10] Li, Z., M.-H. Kim, C. Wang, Z. Han, S. Shrestha, A. C. Overvig, M. Lu, A. Stein, A. M. Agarwal, M. Lončar, and N. Yu, "Controlling propagation and coupling of waveguide modes using phase-gradient metasurfaces," *Nature Nanotechnology*, Vol. 12, 675–683, 2017.

[11] Shen, Y., Z. Pei, Y. Pang, J. Wang, A. Zhang, and S. Qu, "Phase random metasurfaces for broadband wide-angle radar cross section reduction," *Microwave and Optical Technology Letters*, Vol. 57, No. 12, 2813–2819, 2015.

[12] Cheng, Y., C. Wu, C. Ge, J. Yang, X. Pei, F. Jia, and R. Gong, "An ultra-thin dual-band phase-gradient metasurface using hybrid resonant structures for backward RCS reduction," *Applied Physics B*, Vol. 123, No. 5, 143, 2017.

[13] Wang, Y., K. Chen, Y. Li, and Q. Cao, "Design of nonresonant metasurfaces for broadband RCS reduction," *IEEE Antennas and Wireless Propagation Letters*, Vol. 20, No. 3, 346–350, 2021.

[14] Zhang, W., Y. Liu, and S. Gong, "Wideband RCS reduction using two dimensional phase gradient metasurface," in *2017 Sixth Asia-Pacific Conference on Antennas and Propagation (APCAP)*, 1–3, Xi'an, China, 2017.

[15] Jia, Y., Y. Liu, W. Zhang, J. Wang, S. Gong, and G. Liao, "High-gain Fabry-Perot antennas with wideband low monostatic RCS using phase gradient metasurface," *IEEE Access*, Vol. 7, 4816–4824, 2019.

[16] Umair, H., T. B. A. Latef, Y. Yamada, T. Hassan, W. N. L. B. W. Mahadi, M. Othman, K. Kamardin, and M. I. Hussein, "Fabry-Perot antenna employing artificial magnetic conductors and phase gradient metasurface for wideband monostatic RCS reduction and high gain tilted beam radiation," *IEEE Access*, Vol. 9, 66 607–66 625, 2021.

[17] Yu, J., W. Jiang, and S. Gong, "Low-RCS beam-steering antenna based on reconfigurable phase gradient metasurface," *IEEE Antennas and Wireless Propagation Letters*, Vol. 18, No. 10, 2016–2020, 2019.